Composite detrital and thermal remanent magnetization in ash-tuffs from Aeolian Islands (southern Tyrrhenian Sea) revealed by magnetic anisotropy

Elena Zanella[1,2*], Alex Cicchino[1,3], Roberto Lanza[1,2]

Composite detrital and thermal remanent magnetization in tuffs from Aeolian Islands (southern Tyrrhenian Sea) revealed by magnetic anisotropy

[1] Dipartimento di Scienze della Terra, Università di Torino, Via Valperga Caluso 35, 10125 Torino, Italy

[2] ALP – Alpine Laboratory of Paleomagnetism, 12016 Peveragno, Italy

[3] now at Department of Earth Sciences, Durham University, Durham DH1 3LE, UK

[*] corresponding author: elena.zanella@unito.it, ph #390116705165 fax #390116705146

Abstract

This paper reports on the complex relation between rock emplacement and remanence acquisition in tuffs deposited by pyroclastic density currents (PDCs), disclosed by systematic measurements of the anisotropy of magnetic susceptibility (AMS) and natural remanent magnetization (NRM). Thermal demagnetization shows that the NRM consists of two components with different blocking-temperature spectra. The direction of the low-temperature component is consistent with the geocentric axial dipole value, whereas the high-temperature component has dispersed directions. The magnetic fabric is oblate, the magnetic foliation is close to the bedding and the lineations are generally dispersed along a girdle within the foliation plane. The directions of the magnetic lineation and the high-temperature remanence component of individual specimens are close to each other. This correspondence suggests that the high blocking-temperature grains acquired a remanence aligned to their long dimension before deposition, while cooling within the explosive cloud and the moving pyroclastic current. Thereafter, during deposition the traction processes at the base of the current oriented the grains along the flow direction and affected both fabric and high-temperature remanence. This NRM component results from mechanical orientation of previously magnetized grains and is thus detrital in origin. A second, thermal component was then acquired during the cooling of the low blocking-temperature grains after deposition. These results show that NRM in fine-grained pyroclastic rocks is affected by the Earth's magnetic field as

well as the emplacement processes and that magnetic fabric data are essential to unravel its complex nature.

Key words: magnetic fabric, remanent magnetization, pyroclastic rocks

Introduction

The primary remanent magnetization of volcanic rocks is typically thermal (TRM) in origin. It is acquired as the rock cools through the Curie point (T_c) of its ferromagnetic minerals and passes through the blocking temperature T_b spectrum of its ferromagnetic grains. This simple model fully applies to lavas. The temperature of the molten magma is much higher than the Curie point of Ti-magnetite ($T_c \leq 575$ °C), by far the most widespread primary ferromagnetic mineral in volcanic rocks. A lava flow thus acquires a magnetic remanence when cooling after movement has stopped and the two processes are distinct in time. Emplacement of pyroclastic rocks occurs at temperatures that may be as high as for lavas (e.g. fall-out scoriae) and as low as ambient temperature (e.g. lahars), and, in many cases, a substantial cooling occurs while particles are still moving, as in the case of pyroclastic density currents (PDCs) (Cioni et al., 2004; Zanella et al., 2007). Calling deposition temperature (T_{dep}) the temperature at the very moment the pyroclastic material stops moving, two fractions of ferromagnetic grains in principle occur in the rock: those characterized by $T_b > T_{dep}$, which already carry a remanent magnetization as they deposit, and those with $T_b < T_{dep}$, which acquire a TRM as they cool after deposition. The rock's natural remanent magnetization (NRM) consists therefore of a high-temperature component, acquired during the emplacement, and a low-temperature component, acquired during cooling after deposition. The time interval between the acquisition of the two components is so small with respect to the secular variation of the Earth's magnetic field that they are expected to have the same direction and be therefore hardly distinguishable. The composite nature of the NRM in pyroclastic rocks has therefore been overlooked in most paleomagnetic studies.

This paper reports on the case history of Brown Tuffs, a series of tuffs cropping out in the Aeolian Islands (southern Tyrrhenian Sea, Italy), where combination of anisotropy of magnetic susceptibility (AMS) and NRM measurements provides essential information on the timing of remanence acquisition.

Geological setting and sampling

The Brown Tuffs are a sequence of ash-deposits emplaced in the seven islands of the Aeolian archipelago by distinct eruptions that occurred in the last 80 kyr. On the basis of two widespread

tephra layers, they have been divided into three successions, known as Lower (emplaced between 80 and 56 ka), Intermediate (between 56 and 20-22 ka) and Upper (between 20-22 and 4-5 ka) Brown Tuffs (Lucchi et al., 2008). Their lithological, sedimentological and compositional features are similar, irrespective of the age and the geographical distribution of the deposits (De Astis et al. 1997; Lucchi et al. 2008). The Brown Tuffs consist of massive, brown to red, no stratified fine-grained ash, with local discontinuous bedding surfaces and internal banding. The grains mainly consist of juvenile glassy and crystal fragments with minor (≈ 5%) lithic content, and their size is from fine (<0.064 mm) to coarse ash (0.064-2 mm). The crystals are represented by clinopyroxene, plagioclase and minor amounts of olivine and Fe-Ti oxides. Distinct depositional units within the sequence, a few decimeters up to 2-3 m thick, may be identified on the basis of interbedded tephra layers, volcaniclastic deposits and paleosols (De Astis et al. 1997; Lucchi et al. 2008). The Brown Tuffs were emplaced by PDCs: the ash particles were transported by turbulent suspension and deposited at the very base of the current, under the effect of the traction processes exerted by the overlying flow.

A paleomagnetic, rock-magnetic and volcanological investigation has been done to contribute to the between-islands stratigraphical correlation and chronology of the Brown Tuffs units, the results of which are reported in a comprehensive paper (Cicchino et al. in preparation). Here we present the results from selected sites on Lipari and Vulcano islands (Fig. 1) that are useful to understand the effects that the magnetic anisotropy exerts on NRM. At each site, eight to fifteen cores were drilled and oriented with both magnetic and solar compass, collected and then cut to standard (Φ = 24.5 mm, h = 23 mm) cylindrical specimens in the laboratory.

Measurements and results

All measurements were made at the ALP Laboratory (Peveragno, Italy) using a KLY-3 Kappabridge and a JR-6 spinner magnetometer. A Schoenstedt furnace and a Molspin demagnetizer were used for thermal and AF demagnetization, and a PUM pulse magnet for isothermal remanence (IRM) acquisition. Paleomac (Cogné 2003) and Anisoft 4.2 (Chadima and Jelinek 2008) programs were used for data elaboration.

AMS measurements (Table 1) show that the bulk susceptibility value is rather high (K_m = 14,000 ± 5,000 μSI) and the anisotropy degree low (P < 1.030). The geometry of the fabric, however, is well defined and typically oblate. The magnetic foliation is well developed (Fig. 2), whereas lineations are either grouped or dispersed along a girdle within the foliation plane. The main ferromagnetic (*s.l.*) mineral in the Brown Tuffs is Ti-magnetite (Losito 1989; Zanella et al. 1999; Cicchino 2007) and no evidence for other minerals was found in the present investigation.

Interpretation of the AMS fabric of a Ti-magnetite bearing rock requires further information on the magnetic state of the grains, as the AMS maximum axis (K_1) of an unequant grain is parallel to its longest or shortest dimension depending upon wheter the grain is multi- or single-domain respectively. This problem was investigated by measuring anisotropy of remanence, since the maximum axis of remanence is always parallel to the longest dimension of a grain. Anisotropy of isothermal remanent magnetization (AIRM) was therefore measured in some specimens. They were first tumbling demagnetized at 60 mT, then given a steady field of 20 mT and the acquired IRM was measured. These steps were repeated in twelve different sample orientations according to the procedure suggested by Jelinek (1996), in order to cancel out any possible NRM component with coercivity higher than 60 mT, which could bias the IRM measurement. The results show that the three principal IRM and susceptibility axes fall close to each other (Fig. 3). The consistency between AMS and AIRM measurements shows that both maximum axes (K_1 and I_1) match the longest dimension of grains and the magnetic fabric of a specimen can therefore be interpreted as the result of preferential orientation of the longest direction of individual grains. Occurrence of a well developed magnetic foliation shows that the deposition process was highly effective in orienting the longest dimensions of the grains parallel to the bedding plane, yet only in few cases enough to fully align them to a single direction. At most sites, the magnetic lineations are randomly distributed within the foliation plane (Fig. 2b), and we shall see below that this dispersion is relevant to the magnetic remanence of the deposits.

A series of selected specimens was stepwise demagnetized by either thermal or AF methods. A negligible magnetization component of probable viscous origin (VRM) was erased in the first steps. Thermal demagnetization reveals a large (80-90 % of initial NRM) low-temperature (low-T) and a small high-temperature (high-T) component, clearly shown in the Zijderveld (1967) diagram and equal-area projection (Fig. 4a, b, c). As demagnetization proceeds, the measured direction moves along a great circle and points to an overlap of the T_b spectra of the low- and high-T components. AF demagnetization usually fails to pick out the two components (Fig. 4d). Thermal demagnetization was therefore systematically applied to all specimens, heating at 30-40 °C steps. Bulk susceptibility checked after each step showed that no major changes occurred due to heating. Analysis of the results at the site level shows that the attitude of the great circle varies from one specimen to another (Fig. 5) and the great circles intersection yields a statistically significant mean direction (D = 4.4°, I = 53.9°, Fisher (1954) precision k = 145, α_{95}= 3.8°). This means that in each individual specimen a high-T component with variable direction occurs together with a low-T component whose direction is the same in all specimens. This interpretation is further substantiated by the results from site VBT15, where the two components could be separated (Fig. 6) in six

specimens. The high-T directions are dispersed, yet they fall along a great circle that crosses the 95% ellipse of confidence of the site mean value (D = 343.4°, I = 57.2°, k = 147, α_{95}= 5.5°) of the well-grouped low-T directions. This direction, as well as the low-T directions from the other sites (Table 1), is close to the geocentric axial dipole (GAD) value for the Aeolian Islands (D = 0°, I = 59°) and fully consistent with the paleosecular variation changes around it (Zanella, 1995; Lanza and Zanella, 2003).

Joint examination of the AMS and TRM results shows that the maximum anisotropy axis, K_1, of a specimen falls on, or close to, its remagnetization great circle and the remanence direction measured after each step moves toward K_1 as heating proceeds (Fig. 7). We conclude that the K_1 axis of the magnetic fabric biases the direction of the high-T remanence component. This is also clear at the site level. Here, the intersection of the specimens' great circles yields a well defined common direction whereas their dispersion mimics that of the K_1 axes (Fig. 5).

Finally, in the few cases lithic clasts large enough to be measured are embedded in the Brown Tuffs deposits, as at site VBT15 (Fig. 1), the T_{dep} value has been estimated according to the procedure by Cioni et al. (2004). Comparison of thermal demagnetization diagrams (Fig. 8) shows that the reheating ranges of the lithic clasts carried by the PDC and the derived T_{dep} value are consistent with the temperature threshold between the high-T and low-T components of fine-grained tuff. That means that, at the moment of deposition, the decreasing temperature of the cooling ash and the increasing temperature of the warming lithic clasts were similar and corresponded to the deposition temperature. The T_{dep} value falls in the range 320-360 °C at site VBT15, and varies from 280 °C to 360 °C at the other sites.

Discussion and conclusions

The NRM of the Brown Tuffs deposits is carried by primary Ti-magnetite grains and can be regarded as primary in origin because there is no evidence for secondary chemical or thermal processes in the rock. This remanence, however, consists of two components with different directions. The difference cannot result from mechanical deformation due to the load of the overlying deposits because it would have affected the grains carrying both components. Moreover, the thickness of individual Brown Tuffs levels is small (up to a few meters maximum) and the two components occur irrespective of the deposits age, both in the young Upper Brown Tuffs (< 20-22 ka) with little or no overburden as well as in the older Intermediate Brown Tuffs (> 20-22 ka), which in some sections are overlain by the thick pyroclastic deposits of the Monte Guardia sequence.

We are thus confronted with the problem of two magnetizations acquired at the same (geological) time along two distinct directions. Thermal demagnetization shows that the T_b spectra of the two magnetizations are different, even if overlapping, and the direction of the high-T magnetization is deflected toward the AMS maximum axis, K_1. All these results concur to model the NRM acquisition process. The hot grains started to cool down within the explosive cloud and the moving pyroclastic current and, in the absence of external constraints, the high-T_b grains acquired a remanence along the easy magnetization long axis. This process continued until the suspended ash in the flow deposited and the shear exerted by the overlying part aligned the long axes of the grains to the flow direction. The coherent orientation of the grains resulted in the preferential direction of both the rock's fabric and high-T_b remanence. During the eventual cooling below the deposition temperature T_{dep}, the low-T_b grains acquired a remanence along the direction of the Earth's magnetic field. Rock's NRM consists of two components with different origin. An independent evidence of the T_{dep} value is given by the reheating temperatures of the embedded lithic clasts, when available.

According to the model, the high-T_b magnetization component ($T_b > T_{dep}$) of the Brown Tuffs ash deposits is mainly controlled by the depositional dynamics and thus detrital (DRM) in origin, whereas the low-T_b component ($T_b < T_{dep}$) is thermal (TRM), as usual in cooling deposits. The importance of deposition temperature in the magnetic remanence acquisition of pyroclastic rocks was first stressed by Aramaki and Akimoto (1957). Their simple model was based on the consistency of the remanence directions of lithic fragments contained in the deposit: deposition has occurred beyond the Curie point if the directions are uniform, below if they are random. The present model takes into account the T_b spectrum of the fine-grained matrix and thus allows a closer definition of the relation between rock emplacement and remanence acquisition.

Two main conclusions come from the Brown Tuffs test case:

1) paleomagnetic investigation of fine-grained pyroclastic rocks should always be preceded by AMS measurements, in order to assess the possible effects the magnetic fabric has exerted on the NRM;

2) the usual standard to regard the more stable NRM component as the ChRM, i.e. as the characteristic magnetization carrying the direction of the paleofield, could fail when the deposition temperature T_{dep} falls within the T_b spectrum of the rock. In this case, the paleomagnetic information is carried by the component acquired below T_{dep}, whereas the component acquired at higher temperature is related to the emplacement processes.

Acknowledgements

We gratefully acknowledge G. De Astis, F. Lucchi and C. Tranne for passing onto us their deep knowledge of Brown Tuffs and the many enjoyable days spent in the field. The paper benefited by thorough revision and useful comments by M. Ort and M. Porreca. Research funded by the INGV-DPC 2004–2006 project, sub-Project V3_5 - Vulcano (G. De Astis, M. Piochi).

References

Aramaki S, Akimoto S (1957) Temperature estimation of pyroclastic deposits by natural remanent magnetism. Am J Sci 255:619-627.

Chadima M, Jelinek V (2008) Anisoft 4.2 Anisotropy data browser. Contrib. Geophys. Geod. 38: 41.

Cicchino A (2007) Studio paleomagnetico dei depositi di Brown Tuff dell'isola di Lipari. M.Sc thesis, University of Torino.

Cioni R, Gurioli L, Lanza R, Zanella E (2004) Temperatures of the A.D. 79 pyroclastic density current deposits (Vesuvius, Italy). J Geophys Res doi: 10.1029/2002JB002251.

Cogne´ J P (2003) PaleoMac: A Macintosh TM application for treating paleomagnetic data and making plate reconstructions. Geochem Geophys Geosyst doi:10.1029/2001GC000227.

De Astis G, Dellino P, De Rosa R., La Volpe L (1997) Eruptive and emplacement mechanisms of widespread fine-grained pyroclastic deposits on Vulcano island (Italy). Bull Volcanol 59:87-102.

Fisher RA (1953) Dispersion on a sphere. Proc R Soc 217:295-305.

Halls H C (1978) The use of converging remagnetization circles in paleomagnetism. Phys Earth Planet Inter 16:1-11.

Jelinek V (1977) The statistical theory of measuring anisotropy of magnetic susceptibility of rocks and its application. Geofyzika: 1–88.

Jelinek V (1996) Theory and measurements of the anisotropy of isothermal remanent magnetization of rocks. Travaux Géophysiques 37:124-134.

Lanza R, Zanella E (2003) Paleomagnetic secular variation at Vulcano (Aeolian Islands) during the last 135 kyr. Earth Planet Sci Lett 213:321-336.

Losito R 1989 Stratigrafia, caratteri deposizionali e aree sorgente dei Tufi bruni delle isole Eolie. Dissertation, University of Bari.

Lucchi F, Tranne CA, De Astis G, Keller J, Losito R, Morche W (2008) Stratigraphy and significance of Brown Tuffs on the Aeolian islands (southern Italy). J Volcanol Geotherm Res doi: 10.1016/j.jvolgeores.2007.11.006.

McFadden PL, McElhinny MW (1988) The combined analysis of remagnetization circles and direct observations in palaeomagnetism. Earth Planet Sci Lett 87:161-172.

237 Zanella E 1995 Studio delle variazioni paleosecolari del campo magnetico terrestre registrate nelle
238 vulcaniti quaternarie dell'area tirrenica e del Canale Sicilia. Dissertation, University of Torino.
239 Zanella E, De Astis G, Dellino P, Lanza R, La Volpe L (1999) Magnetic fabric and remanent
240 magnetization of pyroclastic surge deposits from Vulcano (Aeolian islands, Italy). J Volcanol
241 Geotherm Res 93:217-236.
242 Zanella E, Gurioli L, Pareschi MT, Lanza R (1997) Influences of urban fabric on pyroclastic density
243 currents at Pompeii (Italy): 2. Temperature of the deposits and hazard implications. J Geophys Res
244 112 doi: 10.1029/2006JB004775.
245 Zijderveld JDA (1967) AC demagnetization of rocks: analysis of results. In: Runcorn SK, Creer
246 KM. Collinson DW (eds) Methods in paleomagnetism, Elsevier, Amsterdam: 254-286.
247

Figure captions

Fig. 1 Geological sketch map of Lipari and Vulcano, Aeolian Islands (courtesy F. Lucchi). Acronyms: UBT / IBT / LBT = Upper / Intermediate / Lower Brown Tuffs. Symbols: square = fine-grained tuff sampling site; dot = fine grained tuff + lithic clasts sampling site.

Fig. 2 Magnetic fabric of the Brown Tuffs: equal-area projection of the principal susceptibility axes. Symbols: square = maximum axis, K_1; triangle = intermediate axis, K_2; dot = minimum axis, K_3; large symbol: site mean value (Jelinek 1977) with 95% ellipse of confidence; great circle = magnetic foliation.

Fig. 3 Equal-area projection of principal susceptibility (a) and isothermal remanence (b) axes at site LBT5. Symbols: square = maximum axis (K_1, I_1); triangle = intermediate axis (K_2, I_2); dot = minimum axis (K_3, I_3); large symbol: site mean value with 95% ellipse of confidence.

Fig. 4 Stepwise thermal (a, b, c) and AF (d) demagnetization. Left: normalized intensity decay curve. Middle: Zijderveld diagram; symbols: full/open dot = declination/apparent inclination. Right: equal-area projection; symbols: full/open dot = positive/negative inclination.

Fig. 5 Equal-area projection of thermal demagnetization results and magnetic lineation at site LBT5. Symbols: great circle = remagnetization circle (Halls 1978); star = site mean value with 95% ellipse confidence; square = magnetic lineation. Figures refer to individual specimens.

Fig. 6 Equal-area projection of thermal demagnetization results at site VBT15. Symbols: dots + great circle = high-T directions + best fitting plane (McFadden and McElhinny 1988); square = site mean low-T direction with 95% ellipse of confidence.

Fig. 7 Equal-area projection of remanence direction during stepwise thermal demagnetization and magnetic lineation. Symbols: dot = remanence direction; square = magnetic lineation, k_1; full/open symbol = positive/negative inclination. The arrow points towards increasing temperature values.

Fig. 8 Deposition temperature of Brown Tuffs deposits at site VBT15. Thermal demagnetization of a fine-grained tuff (a) and an embedded lithic clast (b); symbols as in Fig. 4. Determination of T_{dep}:

horizontal bar = reheating range; stippled area = overlapping of ranges of individual clasts (see Cioni et al., 2004, for further explanation).

Table caption

Table 1 Site mean susceptibility and remanence data. Columns: n = number of specimens; K_m = bulk susceptibility; P = degree of anisotropy; K_1, K_3 = maximum, minimum susceptibility axes: D = declination, I = inclination, E_{1-2}, E_{1-3} = K_1 95% confidence angles, E_{3-2}, E_{3-1} = K_3 95% confidence angles; J_r = NRM intensity; Low-T component: D = declination, I = inclination, *k* = Fisher's (1954) precision, α_{95} = 95% semi-angle of confidence.

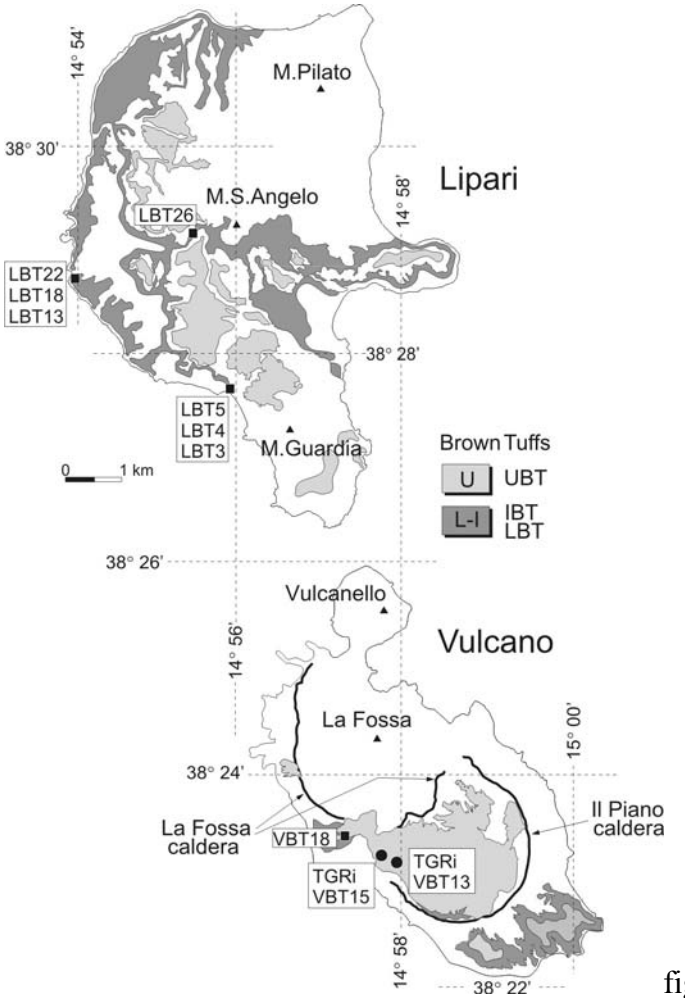

fig.1

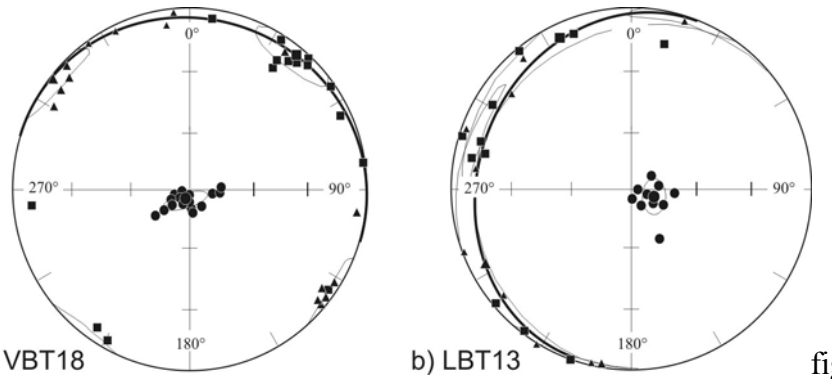
0°
270°
90°
180°
a) VBT18
0°
270°
90°
180°
b) LBT13

fig.2

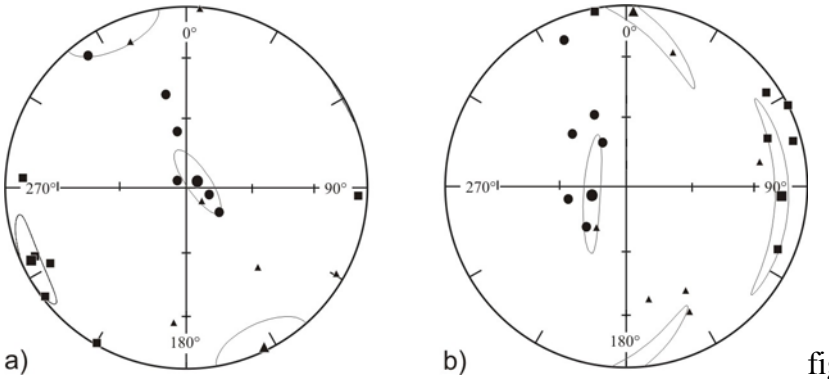
0°
270°
90°
180°
a)
0°
270°
90°
180°
b)

fig.3

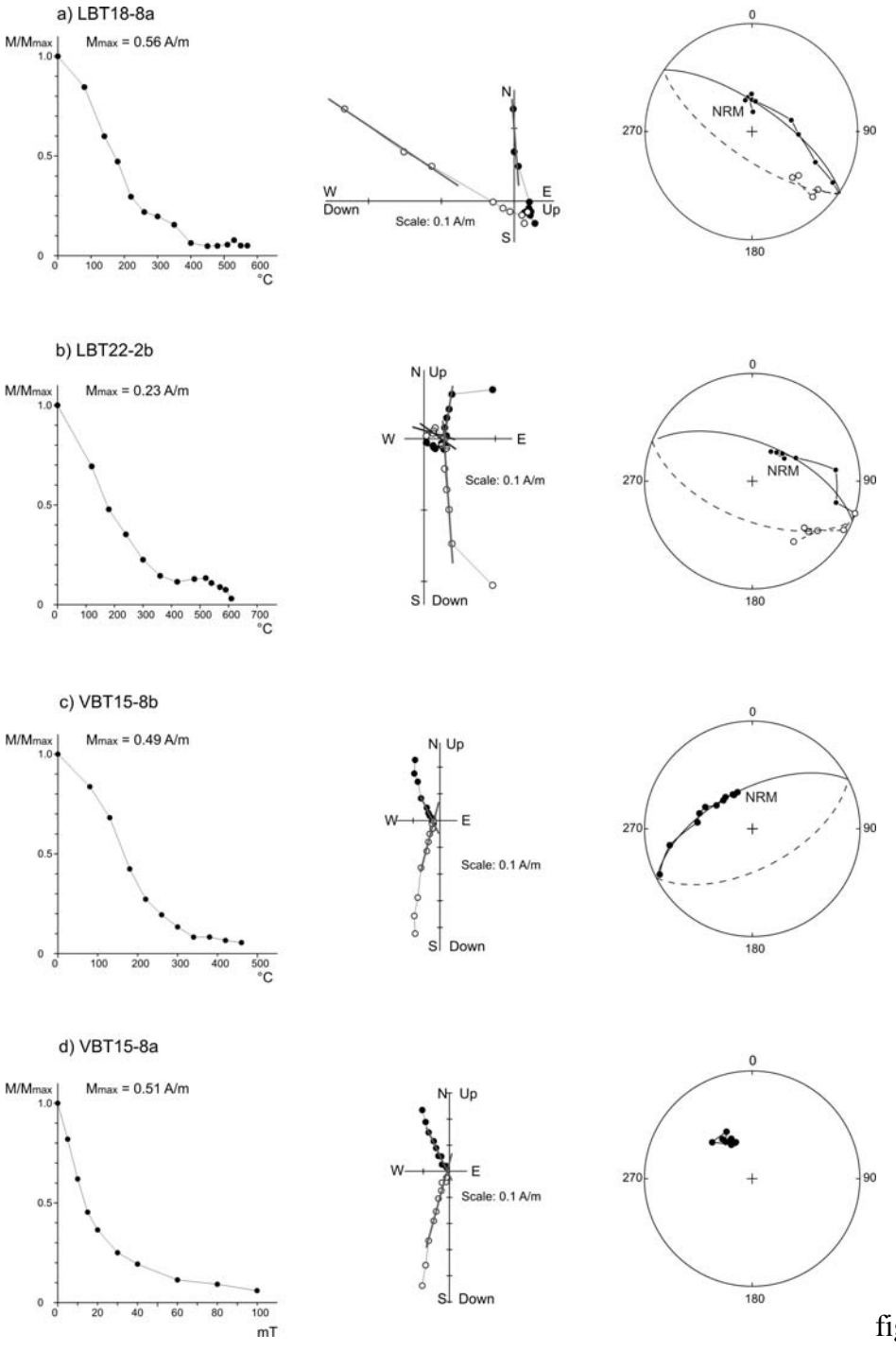
a) LBT18-8a
M/Mmax
Mmax = 0.56 A/m
1.0
0.5
0
0 100 200 300 400 500 600
°C
N
W
E
Down
Up
Scale: 0.1 A/m
S
0
270
90
180
NRM
b) LBT22-2b
M/Mmax
Mmax = 0.23 A/m
1.0
0.5
0
0 100 200 300 400 500 600 700
°C
N Up
W
E
Scale: 0.1 A/m
S Down
0
270
90
180
NRM
c) VBT15-8b
M/Mmax
Mmax = 0.49 A/m
1.0
0.5
0
0 100 200 300 400 500
°C
N Up
W
E
Scale: 0.1 A/m
S Down
0
270
90
180
NRM
d) VBT15-8a
M/Mmax
Mmax = 0.51 A/m
1.0
0.5
0
0 20 40 60 80 100
mT
N Up
W
E
Scale: 0.1 A/m
S Down
0
270
90
180

298 fig.4

299

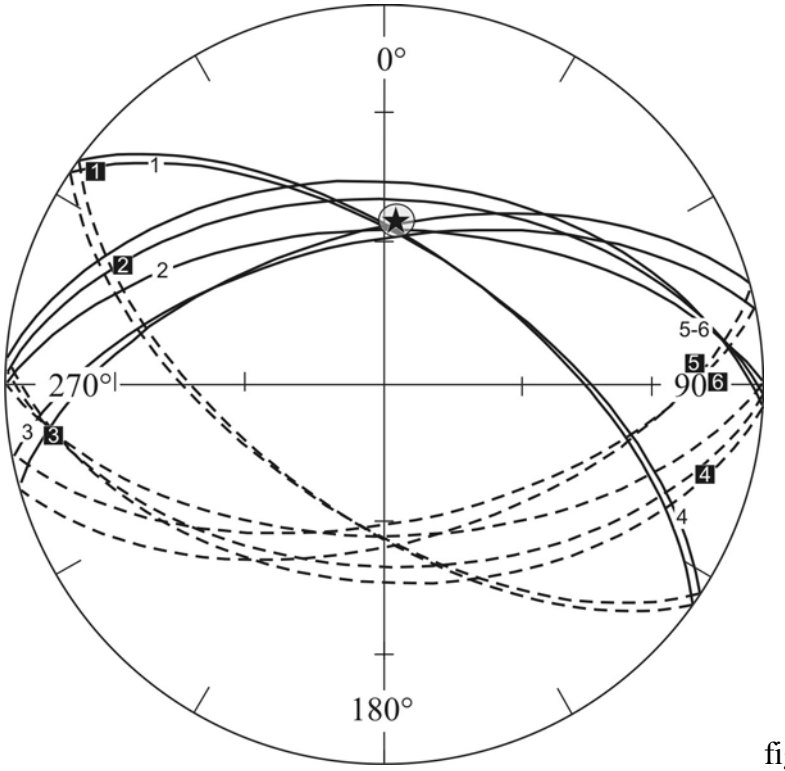

fig.5

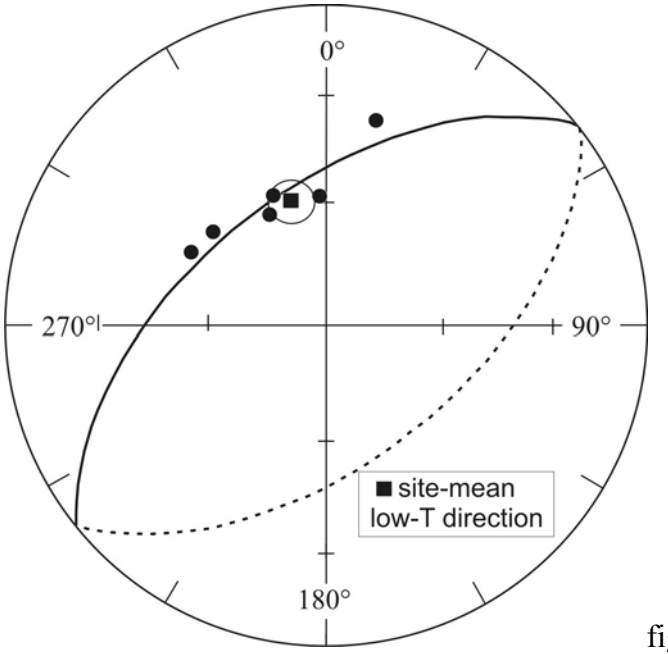

fig.6

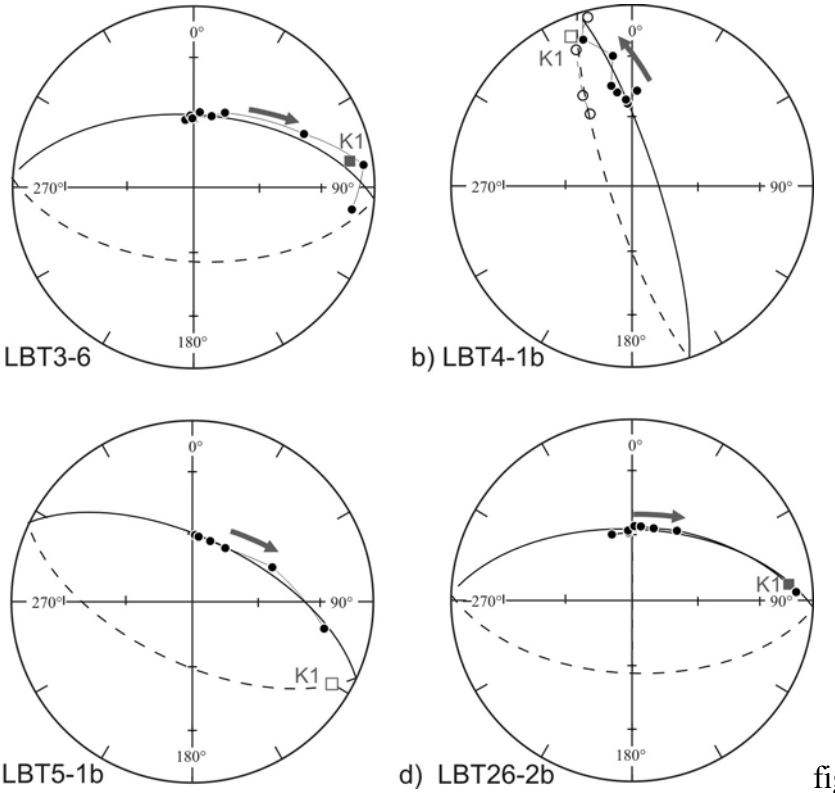

304 fig.7

305

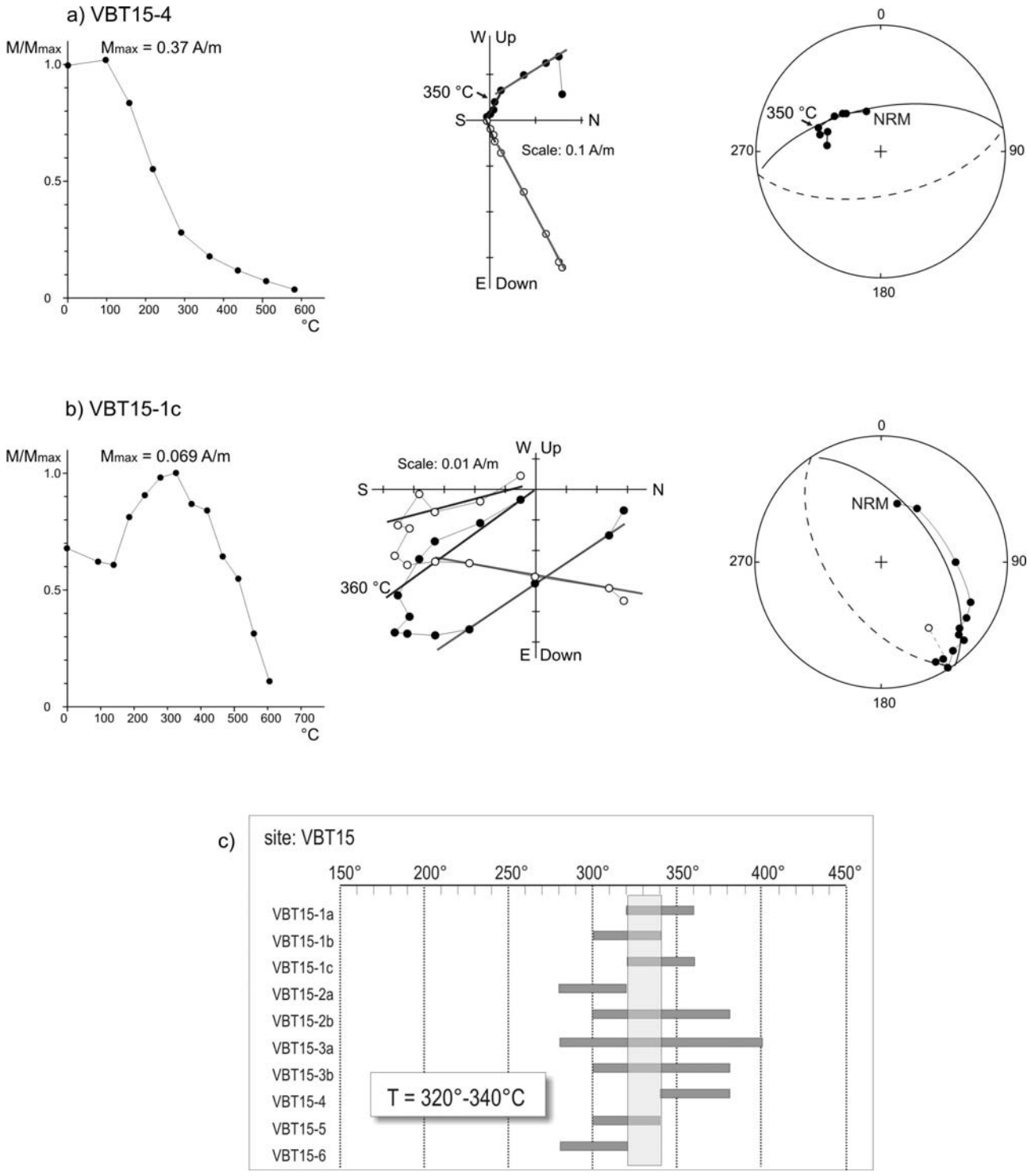
a) VBT15-4
M/Mmax
Mmax = 0.37 A/m
1.0
0.5
0
0 100 200 300 400 500 600
°C
W Up
350 °C
S
N
Scale: 0.1 A/m
E Down
0
350 °C
NRM
270
90
180
b) VBT15-1c
M/Mmax
Mmax = 0.069 A/m
1.0
0.5
0
0 100 200 300 400 500 600 700
°C
W Up
Scale: 0.01 A/m
S
N
360 °C
E Down
0
NRM
270
90
180
c)
site: VBT15
150° 200° 250° 300° 350° 400° 450°
VBT15-1a
VBT15-1b
VBT15-1c
VBT15-2a
VBT15-2b
VBT15-3a
VBT15-3b
VBT15-4
VBT15-5
VBT15-6
T = 320°-340°C

Fig.8

314

Level	n	K_m	P	K_1				K_3				n	Jr	Low-T component			
		(μSI)		D	I	E_{1-2}	E_{1-3}	D	I	E_{3-2}	E_{3-1}		A/m	D	I	*k*	α_{95}
LBT3	11	15180	1.010	227	53	15.5	13.9	119	13	54.6	15.0	11	0.73	6.8	52.6	162	3.8
LBT4	11	17100	1.011	89	12	11.0	5.2	230	74	7.0	5.2	14	0.81	353.8	48.3	59	5.3
LBT5	10	16620	1.013	112	1	27.7	16.1	335	89	24.5	12.5	12	0.98	4.4	53.9	145	3.8
LBT13	10	13550	1.003	334	7	66.3	7.0	109	80	7.6	5.4	8	0.52	14.1	36.0	68	7.2
LBT18	13	19240	1.002	144	16	40.9	31.1	313	74	60.5	30.4	13	0.66	3.2	51.3	134	3.7
LBT22	9	15050	1.007	350	10	53.0	10.2	125	76	18.1	4.1	9	0.66	11.3	57.6	168	4.1
LBT26	20	18270	1.018	115	8	36.0	6.4	328	81	22.6	6.9	19	0.49	357.0	56.8	288	2.0
VBT13	9	13240	1.020	246	29	44.7	28.4	94	58	33.9	58.4	7	0.18	346.2	69.0	105	6.9
VBT15	16	12720	1.003	136	23	53.0	19.6	287	64	22.1	19.8	10	0.36	333.3	56.4	140	4.1
VBT18	16	11720	1.043	38	5	15.2	8.9	197	85	10.4	2.9	7	0.14	328.7	64.4	238	4.1

315 Table1